

Ba₈CoNb₆O₂₄: a spin-1/2 triangular-lattice Heisenberg antiferromagnet in the 2D limit

R. Rawl,¹ L. Ge,² H. Agrawal,³ Y. Kamiya,⁴ C. R. Dela Cruz,³ N. P. Butch,⁵ X. F. Sun,^{6,7,8} M. Lee,^{9,10}
E. S. Choi,¹⁰ J. Oitmaa,¹¹ C. D. Batista,^{1,12} M. Mourigal,^{2,*} H. D. Zhou,^{1,10,†} and J. Ma^{13,1,‡}

¹Department of Physics and Astronomy, University of Tennessee, Knoxville, Tennessee 37996, USA

²School of Physics, Georgia Institute of Technology, Atlanta, GA 30332, USA

³Quantum Condensed Matter Division, Oak Ridge National Laboratory, Oak Ridge, Tennessee 37831, USA

⁴Condensed Matter Theory Laboratory, RIKEN, Wako, Saitama 351-0198, Japan

⁵NIST Centre for Neutron Research, National Institute of Standards and Technology, Gaithersburg, MD 20899, USA

⁶Hefei National Laboratory for Physical Sciences at Microscale,
University of Science and Technology of China, Hefei, Anhui 230026, People's Republic of China

⁷Key Laboratory of Strongly-Coupled Quantum Matter Physics,
Chinese Academy of Sciences, Hefei, Anhui 230026, People's Republic of China

⁸Collaborative Innovation Center of Advanced Microstructures, Nanjing, Jiangsu 210093, People's Republic of China

⁹Department of Physics, Florida State University, Tallahassee, FL 32306, USA

¹⁰National High Magnetic Field Laboratory, Florida State University, Tallahassee, FL 32310, USA

¹¹School of Physics, The University of New South Wales, Sydney, NSW 2052, Australia

¹²Quantum Condensed Matter Division and Shull-Wollan Center,
Oak Ridge National Laboratory, Oak Ridge, Tennessee 37831, USA

¹³Department of Physics and Astronomy, Shanghai Jiao Tong University, Shanghai 200240, China

(Dated: May 17, 2018)

The perovskite Ba₈CoNb₆O₂₄ comprises equilateral effective spin-1/2 Co²⁺ triangular layers separated by six non-magnetic layers. Susceptibility, specific heat and neutron scattering measurements combined with high-temperature series expansions and spin-wave calculations confirm that Ba₈CoNb₆O₂₄ is basically a two-dimensional (2D) magnet with no detectable spin anisotropy and no long-range magnetic ordering down to 0.06 K. In other words, Ba₈CoNb₆O₂₄ is very close to be a realization of the paradigmatic spin-1/2 triangular Heisenberg model, which is not expected to exhibit symmetry breaking at finite temperature according to the Mermin and Wagner theorem.

PACS numbers: 61.05.F-, 75.10.Jm, 75.45.+j, 78.70.Nx

In a celebrated 1966 paper [1], Mermin and Wagner demonstrated that thermal fluctuations prevent 2D magnets to spontaneously break their continuous spin-rotation symmetry if the interactions decay fast enough with the distance between spins. The role of thermal fluctuations is replaced by quantum fluctuations in one-dimensional (1D) systems at temperature $T = 0$; for instance, the spin-1/2 Heisenberg antiferromagnetic chain does not display long-range magnetic order in the $T = 0$ limit and instead hosts quasi-long-range correlations [2] and fractional spin excitations [3–5]. Quantum fluctuations are also expected to have a strong effect on the ground states of highly frustrated 2D and 3D Mott insulators. Indeed, the realization of *quantum spin-liquids*, quantum-entangled states of matter which do not exhibit magnetic ordering, is a major focus of modern condensed matter physics [6, 7]. While spin-liquids are an extreme case of quantum states of matter, 2D systems that *do* order at $T = 0$ can still exhibit strong deviations from semi-classical behavior. For instance, the elementary excitations of a 2D ordered magnet (magnons) become weakly bonded pairs of fractional excitations near the “quantum melting point” (QMP) that signals the transition into a spin liquid state. A clear indication of proximity to a QMP is a strong suppression of the ordered moment relative to the full moment.

The spin-1/2 2D triangular-lattice Heisenberg antiferromagnet (QTLHAF) displays non-collinear spin-order at $T = 0$

with a relative suppression of the ordered moment of more than 50% [8–13]. This makes it an ideal model for studying the effect of strong quantum fluctuations on the spectrum of magnetic excitations. In real materials, however, weak interlayer interactions and spin or spatial anisotropies are likely present. Even extremely small perturbations are sufficient to induce long-range magnetic order at a sizable Néel temperature T_N , because T_N increases logarithmically in the interlayer-coupling or in the exchange anisotropy [14–18]. This is the case for well-studied compounds comprising transition-metal ions, such as Cs₂CuCl₄ ($T_N = 0.62$ K [19]) and Ba₃CoSb₂O₉ ($T_N = 3.8$ K [20]). Quantum effects remain prominent below T_N and lead to order from disorder phenomena, such as the one third magnetization plateaux [21–23], in the presence of an external magnetic field. A recent inelastic neutron scattering (NS) study of Ba₃CoSb₂O₉ [24] showed that even in presence of sizable perturbations [20, 25–27] relative to the pure QTLHAF, dynamical features are not captured by spin-wave theory (SWT). This observation suggests that alternative theoretical approaches are not only needed to describe spin-liquid states, but also to account for qualitative properties of the excitation spectrum of ordered magnets near their QMP [28, 29].

In this Letter, we introduce Ba₈CoNb₆O₂₄, a new realization of the QTLHAF model obtained from Ba₃CoSb₂O₉ by intercalating non-magnetic layers between the triangular

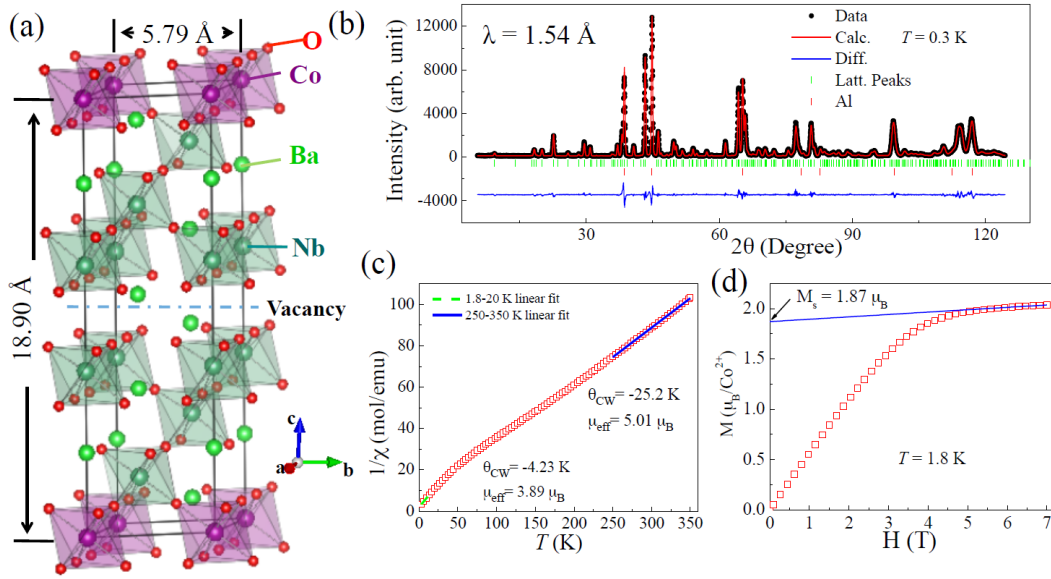


FIG. 1. (color online) (a) Stacked layer structure of $\text{Ba}_8\text{CoNb}_6\text{O}_{24}$ with Co^{2+} ions sitting on a triangular lattice. (b) Rietveld refinement of the neutron powder diffraction pattern measured at $T = 0.3$ K with $\lambda = 1.54$ Å. (c) Temperature dependence of the inverse DC magnetic susceptibility and corresponding Curie-Weiss fits. (d) Isothermal DC magnetization measured at $T = 1.8$ K and extrapolation of the saturated magnetization from the linear dependence above the saturation field (blue solid line).

planes. We present structural, thermo-magnetic, inelastic NS and theoretical results indicating that spin-space anisotropy and inter-plane interactions are both essentially absent in $\text{Ba}_8\text{CoNb}_6\text{O}_{24}$. Having a model realization of the QTL-HAF at hand, we test predictions from semi-classical spin-wave theory and investigate potential exotic phenomena arising from enhanced quantum fluctuations.

To obtain $\text{Ba}_8\text{CoNb}_6\text{O}_{24}$, we start from $\text{Ba}_3\text{CoSb}_2\text{O}_9$, a compound that comprises layers of magnetic CoO_6 octahedral stacked along the hexagonal c axis and separated by two non-magnetic SbO_6 layers. The intra-layer Co–Co distance is 5.86 Å and the interlayer Co–Co distance is 7.23 Å [20]. In the former material, the inter-layer magnetic exchange interaction, J' , is $\sim 5\%$ of the intra-layer exchange J [24, 26]. Moreover, $\text{Ba}_3\text{CoSb}_2\text{O}_9$ possesses a small easy-plane XXZ anisotropy (the ratio between the longitudinal and transverse exchange interactions is $\Delta \approx 0.9$). While the degree of spin anisotropy is difficult to control, one natural strategy to reduce the inter-layer interaction is to insert additional non-magnetic layers in between the magnetic layers. $\text{Ba}_8\text{CoNb}_6\text{O}_{24}$ exactly meets these requirements: it contains a vacant layer and six layers of non-magnetic NbO_6 octahedral between triangular layers of Co^{2+} ions [see Fig. 1(a)]. While the intra-layer Co–Co distance of 5.79 Å is comparable to $\text{Ba}_3\text{CoSb}_2\text{O}_9$, the inter-layer Co–Co distance is dramatically increased up to 18.90 Å [30]. This remarkable structure is expected to guarantee a true 2D nature for the magnetic properties of $\text{Ba}_8\text{CoNb}_6\text{O}_{24}$.

To confirm the physical outcome of our intercalation strategy, we present structural and thermo-magnetic characteriza-

tion of powder samples of $\text{Ba}_8\text{CoNb}_6\text{O}_{24}$ grown from a solid-state synthesis method detailed in the supplemental information (SI) [31]. A fit to our neutron powder diffraction (NPD) pattern measured at $T = 0.3$ K with $\lambda = 1.54$ Å [Fig. 1(b)] yields the space-group $P\bar{3}m1$ with $a = 5.7902(2)$ Å and $c = 18.9026(3)$ Å. A Rietveld refinement yields structural parameters given in SI [31] and indicates a limited amount of disorder ($< 2\%$) between the Co and Nb sites, consistent with an earlier study [30]. The patterns at $T = 0.3$ K and 2.0 K are essentially identical: no additional Bragg peaks appear and broadening of existing peaks is not observed within the sensitivity and resolution of our experiment [31], suggesting the absence of a structural transition or long-range magnetic order down to $T = 0.3$ K.

The temperature dependence of the magnetic DC susceptibility, $\chi(T)$, shows no sign of magnetic ordering or spin freezing down to $T = 1.8$ K [Fig. 1(c)]. The slope of $1/\chi(T)$ changes around $T = 150$ K; Curie-Weiss fits yield $\mu_{\text{eff}} = 5.01(2) \mu_B$ and $\theta_{\text{CW}} = -25.2(3)$ K for $200 \text{ K} < T < 350 \text{ K}$, and $\mu_{\text{eff}} = 3.89(2) \mu_B$ and $\theta_{\text{CW}} = -4.23(1)$ K for $1.8 \text{ K} < T < 30 \text{ K}$. The effective moment reduction indicates a crossover from a high-spin state ($S = 3/2$) to a low-spin state ($S = 1/2$) and is typical for Co^{2+} ions in an octahedral environment, see *e.g.*, ACoB_3 ($A = \text{Cs, Rb}$, $B = \text{Cl, Br}$) [32]. The isothermal DC magnetization at $T = 1.8$ K, shown in Fig. 1(d), indicates that spins saturate above $\mu_0 H_s \approx 4$ T, while a fit to the linear magnetization observed from $\mu_0 H = 5$ T to 7 T uncovers a Van Vleck paramagnetic contribution of $0.023 \mu_B \cdot \text{T}^{-1}$ per Co^{2+} and yields a saturation magnetization $M_s = 1.87 \mu_B$. This value is comparable to that of $\text{Ba}_3\text{CoSb}_2\text{O}_9$ and corre-

sponds to a powder-averaged gyromagnetic ratio $g = 3.84$ for the effective $S = 1/2$ Kramers doublet.

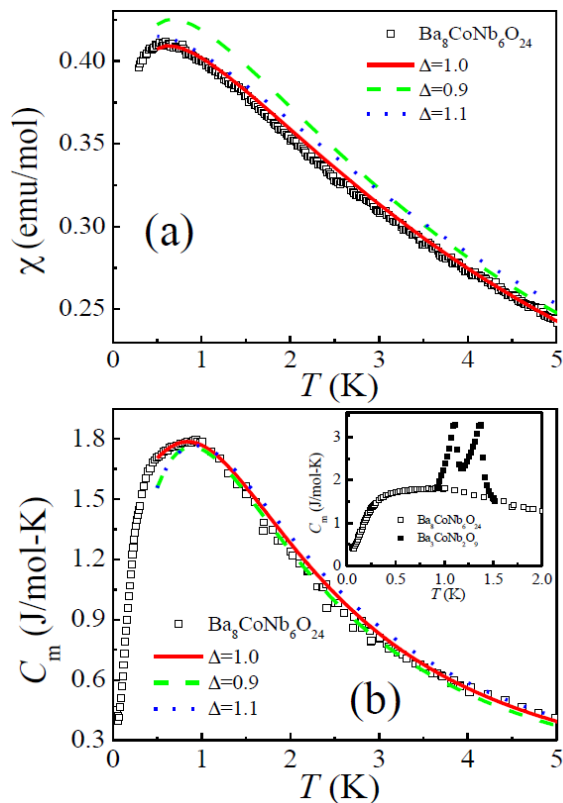


FIG. 2. (color online) (a) Temperature dependence of the magnetic AC susceptibility of $\text{Ba}_8\text{CoNb}_6\text{O}_{24}$ and corresponding high-temperature series expansion simulations for the 2D spin-1/2 triangular-lattice antiferromagnet with XXZ exchange anisotropy. Values of $\Delta = 0.9, 1.0,$ and 1.1 are used and simulations run down to a temperature of 0.5 K using Padé approximants of order [6,6]. The measurements are obtained with an AC excitation field of amplitude 0.5 Oe and frequency 300 Hz, and matched to the DC susceptibility below $T = 15$ K by an overall T -independent rescaling factor [31]. (b) Temperature dependence of the magnetic part of the specific heat of $\text{Ba}_8\text{CoNb}_6\text{O}_{24}$ and matching simulations. (Insert) Comparison to the magnetic specific heat of $\text{Ba}_3\text{CoNb}_2\text{O}_9$.

Similarly, the T -dependence of the magnetic AC susceptibility, shown in Fig. 2(a), uncovers no sharp features down to $T = 0.3$ K. Instead, it reveals a broad peak centered at $T = 0.6$ K, which we associate with the onset of short-range magnetic correlations. The presence of magnetic correlations below $T \approx 1$ K is confirmed by the heat-capacity measurements shown in Fig. 2(b). The magnetic contribution to the specific heat, C_m , was isolated by subtracting the lattice contribution, C_L , of the iso-structural non-magnetic compound $\text{Ba}_8\text{ZnTa}_6\text{O}_{24}$ [31]. The $C_m(T)$ curve reveals a broad peak around $T = 0.8$ K without any sharp feature down to $T = 0.06$ K (the small increase at lower temperatures is attributed to nuclear spins), suggesting the absence of a magnetic phase transition down to $T \leq 0.06$ K. By integrating $C_m(T)/T$

from $T_{\min} = 0.06$ K to a target ($T \leq 8$ K), we obtain the change in magnetic entropy $\Delta S_m = S_m(T) - S_m(T_{\min})$ [31]. The release of entropy reaches $5.32 \text{ J mol}^{-1} \text{ K}^{-1}$ at $T = 8$ K, which is close to the value $R \ln 2 = 5.76 \text{ J mol}^{-1} \text{ K}^{-1}$ expected for a Kramers doublet ground-state.

What is the origin of the broad peak observed in $C_m(T)$? Previous quantum Monte Carlo studies on quasi-2D antiferromagnetic Heisenberg models have shown that the onset of long-range magnetic order yields a sharp peak in $C_m(T)$ even for inter-layer exchange interactions as small as $J'/J = 2 \times 10^{-4}$ [47]. Upon further decreasing the inter-layer coupling, the sharp peak disappears and only a broad peak remains. This is precisely the behavior we observe in $\text{Ba}_8\text{CoNb}_6\text{O}_{24}$, thus exposing the practically ideal 2D nature of magnetism in this compound. This becomes even clearer when our results are compared to $\text{Ba}_3\text{CoNb}_2\text{O}_9$ [see the inset of Fig. 2(b)], which comprises only two non-magnetic layers between the magnetic planes. The specific heat of $\text{Ba}_3\text{CoNb}_2\text{O}_9$ reveals two subsequent phase transitions at $T_{N1} = 1.10$ K and $T_{N2} = 1.36$ K, indicating the presence of easy-axis anisotropy [34]. At a similar energy scale (≈ 1 K), $\text{Ba}_8\text{CoNb}_6\text{O}_{24}$ only exhibits a single broad peak with no observable signs of exchange anisotropy or inter-layer coupling.

The temperature dependence of $\chi(T)$ and $C_m(T)$ for the QTLHAF model has been well documented using high-temperature series expansions (HTSE) [35–38] up to 12th order [46]. To determine if exchange anisotropy is present in $\text{Ba}_8\text{CoNb}_6\text{O}_{24}$, we extend existing HTSE work to the XXZ Hamiltonian,

$$\mathcal{H} = J \sum_{\langle i,j \rangle} (S_i^x S_j^x + S_i^y S_j^y + \Delta S_i^z S_j^z), \quad (1)$$

where $\langle i,j \rangle$ denotes nearest-neighbor spins. We obtained results for the isotropic ($\Delta = 1.0$), easy-plane ($\Delta = 0.9$), and easy-axis ($\Delta = 1.1$) models [31]. The best HTSE fit to our experimental observations, namely $\chi(T)$ and $C_m(T)$ below $T = 5$ K, yields $J = 0.144$ meV for $\Delta = 1.0$ with a fitting error-bar on J smaller than 10^{-3} meV [see Fig. 2]. For a fixed value of J , the fit quality becomes worse as soon as Δ deviates from 1.0 and lead to higher (respectively lower) peak heights for $\chi(T)$ (resp. C_m).

With strong thermodynamic indication that $\text{Ba}_8\text{CoNb}_6\text{O}_{24}$ realizes the purely 2D and spin-isotropic QTLHAF model, we now turn to the nature of its spin excitations. NS intensity (powder-averaged) as a function of momentum transfer Q and energy transfer E allows to track the development of magnetic correlations upon lowering T . In Fig. 3(a), we present such results for $T = 0.3$ K, with additional results for $5 \text{ K} \leq T \leq 0.05$ K included in SI [31]. The momentum dependence of the magnetic signal reveals strong ridges of intensity emerging from $Q \approx 0.7 \text{ \AA}^{-1}$ with less intense repetitions at 1.5 \AA^{-1} and 2.0 \AA^{-1} . While spins appear well-correlated at $T = 0.3$ K, the low-energy signal ($E \leq 0.1$ meV) remains broader than instrumental resolution suggesting that spin correlations remain short-ranged and static magnetic order is absent. The energy dependence of the main signal reveals gap-

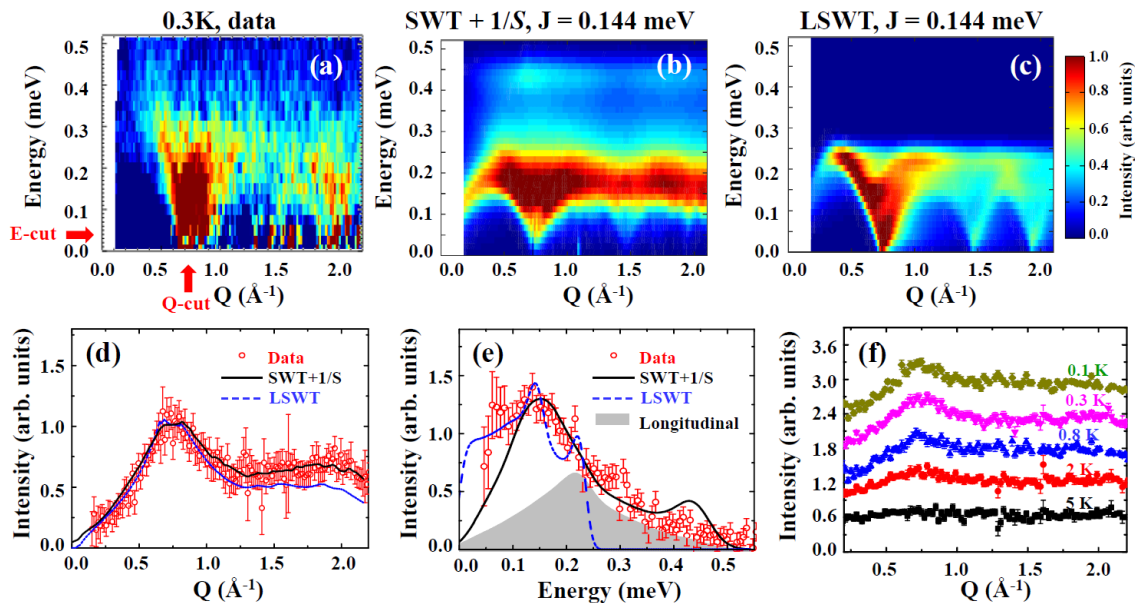


FIG. 3. (color online) (a) Powder-averaged inelastic NS spectra of $\text{Ba}_8\text{CoNb}_6\text{O}_{24}$ at $T = 0.3$ K. Data collected at $T = 10$ K is used as background. (b,c) NS intensity calculated for $J = 0.144$ meV using non-linear SWT with $1/S$ -corrections and linear SWT, respectively. Calculated intensities have been convoluted by Gaussian profiles of full-width at half maximum $\Delta E = 0.025$ meV and $\Delta Q = 0.015 \text{ \AA}^{-1}$ to approximate the effects of instrumental resolution. (d,e) Comparisons between experiment (red dots), $1/S$ -SWT (solid black line) and linear SWT (dashed blue line) as energy-integrated ($0.05 \leq E \leq 0.52$ meV) and momentum-integrated ($0.6 \leq Q \leq 0.9 \text{ \AA}^{-1}$) cuts, respectively. The shaded (gray) area corresponds to the longitudinal (two-magnon) contribution to the NS intensity in $1/S$ -SWT. The high-energy bump around $E = 0.45$ meV in (e) is an artifact of our $1/S$ approximation [40]. (f) Temperature dependence of the energy-integrated intensity of (d). Error bars correspond to one standard error.

less excitations extending up to 0.35 meV with less intense signal reaching up to $E = 0.45$ meV. These features do not change significantly as T is lowered [31].

To model the dynamic magnetic correlations, we resort to SWT at $T = 0$; $1/S$ corrections [40] are included in Fig. 3(b) while we remain strictly at the linear level (LSWT) [48] in Fig. 3(c). We assume that the system orders in the 120° magnetic structure, at least at $T = 0$, and use $J = 0.144$ meV from the thermodynamic measurements. Our E -integrated [Fig. 3(d)] and Q -integrated [Fig. 3(e)] scans reveal a good agreement between NS measurements and powder-averaged $1/S$ -SWT predictions. The most visible improvement between $1/S$ and linear SWT calculations stems from the inclusion of longitudinal spin fluctuations in the former. These excitations reflect the reduction of the ordered moment by quantum fluctuations and form a high-energy continuum also known as two-magnon scattering. The absence of notable temperature dependence for the $E \geq 0.1$ meV magnetic scattering below $T = 0.5$ K [Fig. 3(f)] further supports the evidence for strong quantum fluctuations in the ground-state of $\text{Ba}_8\text{CoNb}_6\text{O}_{24}$.

It is instructive to compare the excitations of $\text{Ba}_8\text{CoNb}_6\text{O}_{24}$ with that of the quasi-2D compound $\text{Ba}_3\text{CoSb}_2\text{O}_9$, for which $J' = 0.05 J$, $J \approx 1.7$ meV, and $\Delta \approx 0.9$. While both compounds comprise structurally similar magnetic layers with comparable Co-Co bond lengths, the ~ 2.0 meV in-plane

excitation bandwidth of $\text{Ba}_3\text{CoSb}_2\text{O}_9$ is an order of magnitude larger than the present observation of ~ 0.18 meV for $\text{Ba}_8\text{CoNb}_6\text{O}_{24}$. In units of their respective J , the bandwidth $W \approx 1.18 J$ for the former compound compares well with $W \approx 1.24 J$ obtained by the present $1/S$ -SWT analysis for $\text{Ba}_8\text{CoNb}_6\text{O}_{24}$ [see Fig. 3(b)]. While $\text{Ba}_3\text{CoSb}_2\text{O}_9$ develops long-range magnetic ordering below $T_N = 3.7$ K $\sim 0.19J$, $\text{Ba}_8\text{CoNb}_6\text{O}_{24}$ does not exhibit any magnetic ordering down to $T = 0.06$ K $\sim 0.04J$. Given that T_N increases logarithmically both in the magnitude of J' and Δ , the suppression of T_N/J by a factor of at least 4 relative to $\text{Ba}_3\text{CoSb}_2\text{O}_9$ implies that inter-plane and anisotropic exchange interactions must be extremely small in $\text{Ba}_8\text{CoNb}_6\text{O}_{24}$.

In conclusion, our powder-sample experiments reveal that $\text{Ba}_8\text{CoNb}_6\text{O}_{24}$ is virtually an ideal realization of the QTL-HAF and a unique compound to expose the consequences of the Mermin and Wagner theorem in a real triangular-lattice material. Recent studies have shown that quantum fluctuations have a non-perturbative effect on the magnetic excitations of quasi-2D quantum antiferromagnets [24, 42]. We expect even stronger quantum effects in the magnetic excitation spectrum of $\text{Ba}_8\text{CoNb}_6\text{O}_{24}$, making it an even better candidate to challenge existing semi-classical theories for the dynamic response of frustrated quantum antiferromagnets. From the materials discovery standpoint, our work devises a method for reducing dimensionality by intercalating non-

magnetic layers in layered compounds that can be extended to other lattices to reveal new physics.

R.R. and H.D.Z. thank the support of NSF-DMR-1350002. J.M. thanks the support of the Ministry of Science and Technology of China (2016YFA0300500). The work at Georgia Tech (L.G., M.M.) was supported by the College of Sciences and ORAU's Ralph E. Powe Junior Faculty Enhancement Award. X.F.S. acknowledges support from the National Natural Science Foundation of China (Grant Nos. 11374277 and U1532147), the National Basic Research Program of China (Grant Nos. 2015CB921201 and 2016YFA0300103), and the Opening Project of Wuhan National High Magnetic Field Center (Grant No. 2015KF21). The work at NHMFL is supported by NSF-DMR-1157490, the State of Florida and the U.S. Department of Energy. The work at ORNL High Flux Isotope Reactor was sponsored by the Scientific User Facilities Division, Office of Basic Energy Sciences, U.S. Department of Energy.

* mourigal@gatech.edu

† hzhou10@utk.edu

‡ jma3@sjtu.edu.cn

- [1] N. D. Mermin and H. Wagner, *Phys. Rev. Lett.* **17**, 1133 (1966).
- [2] E. Lieb, T. Schultz, and D. Mattis, *Ann. Phys.* **16**, 407 (1961).
- [3] L. D. Faddeev and L. A. Takhtajan, *Phys. Lett. A* **85**, 375 (1981).
- [4] D. A. Tennant, T. G. Perring, R. A. Cowley, and S. E. Nagler, *Phys. Rev. Lett.* **70**, 4003 (1993).
- [5] M. Mourigal, M. Enderle, A. Klöpperpieper, J.-S. Caux, A. Stunault, and H. M. Rønnow, *Nature Physics* **9**, 435 (2013).
- [6] L. Savary and L. Balents, arXiv:1601.03742 (2016).
- [7] A. Banerjee, C. A. Bridges, J.-Q. Yan, A. A. Aczel, L. Li, M. B. Stone, G. E. Granroth, M. D. Lumsden, Y. Yiu, J. Knolle, S. Bhattacharjee, D. L. Kovrizhin, R. Moessner, D. A. Tennant, D. G. Mandrus, and S. E. Nagler, *Nature Materials*, doi:10.1038/nmat4604 (2016).
- [8] Th. Jolicoeur and J. C. Le Guillou, *Phys. Rev. B* **40**, 2727 (1989).
- [9] A. V. Chubukov, S. Sachdev, and T. Senthil, *J. Phys: Cond. Matt.* **6**, 8891 (1994).
- [10] L. Capriotti, A. E. Trumper, and S. Sorella, *Phys. Rev. Lett.* **82**, 3899 (1999).
- [11] W. H. Zheng, J. O. Fjærestad, R. R. P. Singh, R. H. McKenzie, and R. Coldea, *Phys. Rev. B* **74**, 224420 (2006).
- [12] S. R. White and A. L. Chernyshev, *Phys. Rev. Lett.* **99**, 127004 (2007).
- [13] A. L. Chernyshev and M. E. Zhitomirsky, *Phys. Rev. B* **79**, 144416 (2009).
- [14] K Hirakawa, *J. Appl. Phys.* **53**, 1893 (1982).
- [15] A. Cuccoli, T. Roscilde, R. Vaia, and P. Verrucchi, *Phys. Rev. Lett.* **90**, 167205 (2003).
- [16] S. Miyashita and H. Kawamura, *J. Phys. Soc. Jpn.* **54**, 3385 (1985).
- [17] W. Stephan and B. W. Southern, *Phys. Rev. B* **61**, 11514 (2000).
- [18] S. Fujimoto, *Phys. Rev. B* **73**, 184401 (2006).
- [19] R. Coldea, D. A. Tennant, R. A. Cowley, D. F. McMorrow, B. Dorner, and Z. Tylczynski, *Phys. Rev. Lett.* **79**, 151 (1997).
- [20] Y. Doi, Y. Hinatsu, and K. Ohoyama, *J. Phys: Cond. Mat.* **16**, 8923 (2004).
- [21] H. Tsujii, C. R. Rotundu, T. Ono, H. Tanaka, B. Andraka, K. Ingersent, and Y. Takano, *Phys. Rev. B* **76**, 060406 (2007).
- [22] W.-J. Hu, S.-S. Gong, W. Zhu, and D. N. Sheng, *Phys. Rev. B* **92**, 140403 (2015).
- [23] G. Koutroulakis, T. Zhou, Y. Kamiya, J. D. Thompson, H. D. Zhou, C. D Batista, and S. E. Brown, *Phys. Rev. B* **91**, 024410 (2015).
- [24] J. Ma, Y. Kamiya, T. Hong, H. B. Cao, G. Ehlers, W. Tian, C. D. Batista, Z. L. Dun, H. D. Zhou, and M. Matsuda, *Phys. Rev. Lett.* **116**, 087201 (2016).
- [25] Y. Shirata, H. Tanaka, A. Matsuo, and K. Kindo, *Phys. Rev. Lett.* **108**, 057205 (2012).
- [26] T. Susuki, N. Kurita, T. Tanaka, H. Nojiri, A. Matsuo, K. Kindo, and H. Tanaka, *Phys. Rev. Lett.* **110**, 267201 (2013).
- [27] N. A. Fortune, S. T. Hannahs, Y. Yoshida, T. E. Sherline, T. Ono, H. Tanaka, and Y. Takano, *Phys. Rev. Lett.* **102**, 257201 (2009).
- [28] H. D. Zhou, C. Xu, A. M. Hallas, H. J. Silverstein, C. R. Wiebe, I. Umegaki, J. Q. Yan, T. P. Murphy, J. -H. Park, Y. Qiu, J. R. D. Copley, J. S. Gardner, and Y. Takano, *Phys. Rev. Lett.* **109**, 267206 (2012).
- [29] E. A. Ghioldi, A. Mezio, L. O. Manuel, R. R. P. Singh, J. Oitmaa, and A. E. Trumper, *Phys. Rev. B* **91**, 134423 (2015).
- [30] P. M. Mallinson, M. M. Allix, J. B. Claridge, R. M. Ibberson, D. M. Iddles, T. Price, and M. J. Rosseinsky, *Angew. Chem Int. Ed.* **44**, 7733 (2005).
- [31] See online supplementary information.
- [32] M. F. Collins and O. A. Petrenko *Can. J. Phys.* **75**, 605 (1997).
- [33] P. Sengupta, A. W. Sandvik, R. R. P. Singh, *Phys. Rev. B* **68**, 094423 (2003).
- [34] M. Lee, J. Hwang, E. S. Choi, J. Ma, C. R. Dela Cruz, M. Zhu, X. Ke, Z. L. Dun, and H. D. Zhou, *Phys. Rev. B* **89**, 104420 (2014).
- [35] N. Chandrasekharan and S. Vasudevan, *Phys. Rev. B* **54**, 14903 (1996).
- [36] H. Rosner, R. R. P. Singh, W. H. Zheng, J. Oitmaa, and W. E. Pickett, *Phys. Rev. B* **67**, 014416 (2003).
- [37] R. R. P. Singh and J. Oitmaa, *Phys. Rev. B* **85**, 104406 (2012).
- [38] J. Oitmaa, C. Hamer, and W. Zheng, *Series Expansion Methods for Strongly Interacting Lattice Models*, (University Press, Cambridge, 2006).
- [39] N. Elstner, R. R. P. Singh, and A. P. Young, *Phys. Rev. Lett.* **71**, 1629 (1993).
- [40] M. Mourigal, W. T. Fuhrman, A. L. Chernyshev, and M. E. Zhitomirsky, *Physical Review B* **88**, 094407 (2013).
- [41] S. Toth and B. Lake, *Journal of Physics: Condensed Matter* **27**, 166002 (2015).
- [42] B. Dalla Piazza, M. Mourigal, N. B. Christensen, G. J. Nilsen, P. Tregenna-Piggott, T. G. Perring, M. Enderle, D. F. McMorrow, D. A. Ivanov, and H. M. Rønnow, *Nature Physics* **11**, 62 (2015).
- [43] Z. L. Dun, E. S. Choi, A. M. Hallas, C. R. Wiebe, J. S. Gardner, E. Arrighi, R. S. Freitas, A. M. Arevalo-Lopez, J. P. Attfield, H. D. Zhou, and J. G. Cheng, *Phys. Rev. B* **89**, 064401 (2014).
- [44] J. Rodriguez-Carvajal, *Physica B* **192**, 55-69 (1993).
- [45] J. R. D. Copley and J. C. Cook, *Chem. Phys.* **292**, 477 (2003).
- [46] N. Elstner, R. R. P. Singh, and A. P. Young, *Phys. Rev. Lett.* **71**, 1629 (1993).
- [47] J. Oitmaa, C. Hamer, and W. Zheng, *Series Expansion Methods for Strongly Interacting Lattice Models*, (University Press, Cambridge, 2006).
- [48] S. Toth and B. Lake, *Journal of Physics: Condensed Matter* **27**, 166002 (2015).

Supplementary online material for “Ba₈CoNb₆O₂₄: a spin-1/2 triangular-lattice Heisenberg antiferromagnet in the 2D limit”

Experimental details—Ba₈CoNb₆O₂₄ was synthesized using solid state reactions by mixing stoichiometric ratios of BaCO₃, CoCO₃, and Nb₂O₅ and annealing at 1500 °C for 48 hours with one intermediate grinding. The DC susceptibility measurements were taken down to 1.8 K using a commercial superconducting interference device magnetometer (Quantum Design) in a field of 5000 Oe. The AC susceptibility was measured at National High Magnetic Field Laboratory using a homemade setup with AC excitation field 0.5 Oe and frequency 300 Hz [43]. The specific heat was measured down to 0.05 K using a Physical Properties Measurement System of Quantum Design. The neutron powder diffraction (NPD) was carried out down to 0.3 K on HB-2A neutron powder diffractometer at Oak Ridge National Laboratory with wavelengths of 1.5406 Å and 2.4111 Å with a collimation of 12'-open-6'. The shorter wavelength gives a greater intensity and higher Q coverage that was used to investigate the crystal structure, while the longer wavelength gives lower Q coverage and greater resolution that was important for investigating the magnetic structures. Rietveld refinement was performed using Fullprof to refine the data [44]. Inelastic neutron scattering (INS) was performed down to 0.06 K at National Institute of Standards and Technology (NIST) CHRNS using the time-of-flight spectrometer, disk chopper spectrometer (DCS) with three wavelengths of 1.8, 5.0, and 7.5 Å [45].

Neutron powder diffraction—Fig. S1(a) shows the neutron powder diffraction patterns measured at 0.3 and 2 K with $\lambda = 2.4111$ Å. There is no resolvable differences between them and thus no signs for long range magnetic ordering (LRO) or structural distortion down to 0.3 K. The lattice parameters and atomic positions refined from 0.3 K data are listed in Table S1.

TABLE S1. Structural parameters for Ba₈CoNb₆O₂₄ at 0.3 K

Refinement	Atom	Site	x	y	z	Occupancy
$\lambda = 1.5404$ Å RF-factor = 2.44 Bragg R-fct = 3.21 <i>P</i> -3 <i>m</i> 1	Ba(1)	2c	0	0	0.18771(36)	1/6
	Ba(2)	2d	1/3	2/3	0.06126(52)	1/6
	Ba(3)	2d	1/3	2/3	0.45478(41)	1/6
	Ba(4)	2d	1/3	2/3	0.68149(32)	1/6
	Co	1a	0	0	0	0.084(2)
	Nb(1)	2c	0	0	0.38677(30)	0.166(1)
	Nb(2)	2d	1/3	2/3	0.25272(33)	0.166(1)
	Nb(3)	2d	1/3	2/3	0.87707(33)	0.166(1)
	O(1)	6i	0.16937(49)	0.30685(19)	0.30685(19)	1/2
	O(2)	6i	0.16413(38)	0.83577(38)	0.56995(19)	1/2
O(3)	6i	0.17068(57)	0.82922(57)	0.93424(26)	1/2	
O(4)	6i	0.49774(61)	0.50216(61)	0.18738(14)	1/2	
$a = 5.7902(2)$ (Å), $c = 18.9026(3)$ (Å)						
Overall B-factor = 0.093(8) (Å ²)						

Magnetic susceptibility scaling—The temperature dependence of the AC susceptibility measured with a small AC field and low frequency should reflect the intrinsic susceptibility behavior of a system, or has the same temperature trend of the DC susceptibility measured on the same system. Therefore, a AC field of 0.5 Oe with frequency 300 Hz was used to measure the magnetic susceptibility down to 0.3 K. This data was easily matched to the high temperature DC susceptibility data taken down to 1.8 K with a simple scaling factor (Fig. S1(b)). As the behaviors between them are essentially identical, the scaled AC data was used for all simulations and fittings to extend the data down to 0.3 K. Unit of the DC susceptibility $\chi = \text{emu/mol}$ is used for scaled AC data to maintain continuity.

Specific heat—The magnetic specific heat for Ba₈CoNb₆O₂₄ was isolated by subtracting a non-magnetic lattice standard, Ba₈ZnTa₆O₂₄ (Fig. S1(c)). Since the high temperature series expansion (HTSE) only provides magnetic contributions to the C_p , the standard subtracted data was used in all fittings and comparisons. The integration of C_p/T between 0.06 and 8 K of the magnetic C_m saturates at $\Delta S = 5.32$ J/mol-K. This value is close to the $R\ln(2) = 5.76$ J/mol-K, which is expected for a spin-1/2 system.

High temperature series expansion—The HTSE was used to obtain the exchange constant and exchange anisotropy of Ba₈CoNb₆O₂₄ in both χ and C_p down to 0.5 K. The coefficients a_n, c_n (Eqs. S1 and S2 respectively) for C_p and χ of the spin-1/2 isotropic Heisenberg TLAf have been calculated up to 12th order in previous work [46]. To analyze the effect of the exchange anisotropy, we computed the coefficients for the spin-1/2 *anisotropic* Heisenberg TLAf for up to 12th order for $\Delta = 0.9, 1.1$ (see Table S2). C_p was calculated from the T -derivative of the free energy given in Eq. S1 and χ was calculated using Eq. S2.

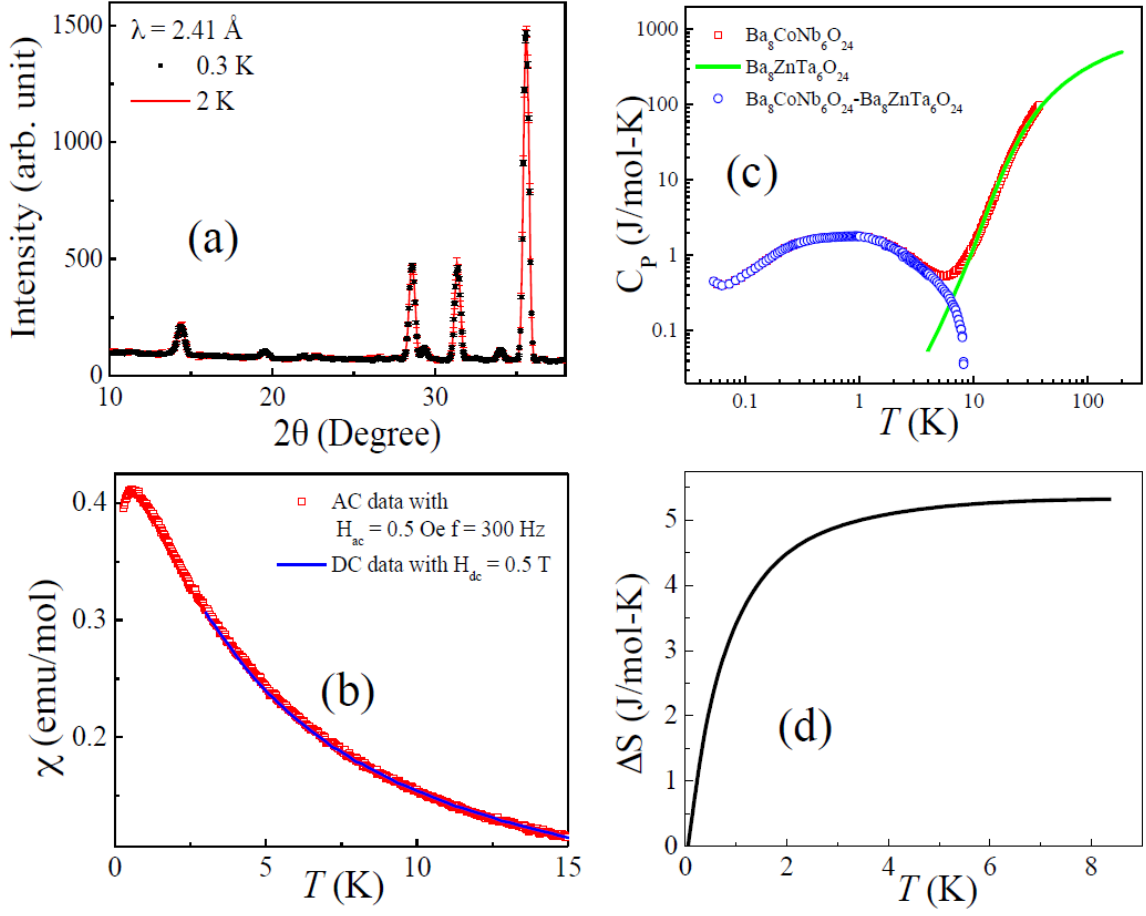


FIG. S1. (color online) (a) The neutron powder diffraction patterns for $\text{Ba}_8\text{CoNb}_6\text{O}_{24}$ taken at 0.3 and 2 K at HB-2A with $\lambda = 2.4111$ Å. (b) The magnetic susceptibility for $\text{Ba}_8\text{CoNb}_6\text{O}_{24}$ shown with DC data and scaled AC data. (c) The specific heat for $\text{Ba}_8\text{CoNb}_6\text{O}_{24}$, $\text{Ba}_8\text{ZnTa}_6\text{O}_{24}$ and the difference taken to isolate the magnetic contribution. (d) The magnetic entropy calculated from integration of C_p/T . Error bars correspond to uncertainties of one standard deviation.

$$\frac{\ln Z}{N} = \sum_{n=0} a_n x^n \quad (\text{S1})$$

$$\frac{k_B T \chi}{(g\mu_B)^2} = \sum_{n=0} c_n x^n \quad (\text{S2})$$

Padé approximants—The low-temperature divergence of the plain HTSE of Eq. S1 can be avoided by using the ratio method, integrated differential approximants, and Padé approximants [47]. For this letter, we use Padé approximants of order $[m = 6, n = 6]$ as originally used by Elstner et al [46] and described in Eq. S3. We chose approximants of order $[6, 6]$ for two reasons. First, C_p being calculated by differentiating free energy results in non-physical divergences at $T = J/k_B$ for some off-diagonal approximants, namely $[7, 5]$ and $[5, 7]$. Second, the diagonal order $[n, n]$ avoids a divergent low-temperature behavior. Other approximants were examined, but Padé approximants of order $[6, 6]$ provide the most physically meaningful results for simulations below $T = J/k_B$.

$$R(x) = \frac{\sum_{j=0}^m a_j x^j}{1 + \sum_{k=1}^n a_k x^k} \quad (\text{S3})$$

Inelastic neutron scattering—Fig. S2 shows the INS spectra measured from 0.06 and 5 K. There is no sign for LRO or structural distortion down to 0.06 K. The magnetic dynamic signal begins to appear around $T = 5$ K. With decreasing

TABLE S2. HTSE coefficients for $\Delta = 0.9, 1.1$

n	$\Delta = 0.9$		$\Delta = 1.1$	
	$\ln Z$	χ	$\ln Z$	χ
0	0.693147180560E+00	0.250000000000E+00	0.693147180560E+00	0.250000000000E+00
1	0.000000000000E+00	-0.135000000000E+01	0.000000000000E+00	-0.165000000000E+01
2	0.421500000000E+01	0.457500000000E+01	0.481500000000E+01	0.757500000000E+01
3	-0.275800000000E+01	-0.928600000000E+01	-0.336200000000E+01	-0.267540000000E+02
4	-0.110157250000E+02	0.735865000000E+01	-0.143937250000E+02	0.833306500000E+02
5	0.227150400000E+02	0.813502200000E+01	0.316609600000E+02	-0.274087222000E+03
6	0.555289564000E+02	-0.432566133333E+01	0.830983377333E+02	0.971839778667E+03
7	-0.230309437387E+03	0.309929443029E+02	-0.367686192480E+03	-0.315219402327E+04
8	-0.251495874650E+03	-0.905870806367E+03	-0.428893232275E+03	0.868118706817E+04
9	0.237935023053E+04	0.359542189692E+04	0.433229044400E+04	-0.243590877456E+05
10	-0.490854208087E+02	-0.374861931449E+02	-0.625397496451E+02	0.877627224099E+05
11	-0.239243887884E+05	-0.309077579057E+05	-0.498804497089E+05	-0.317811658164E+06
12	0.262699694109E+05	0.180327243359E+05	0.582734814011E+05	0.840953315702E+06

temperature, the magnetic spectra becomes more clear. However, the INS spectra does not change below $T = 0.5$ K and the spin-wave is not well formed even at 0.06 K.

Spin-wave theory—The isotropic Hamiltonian with only nearest neighbor exchange interaction $J = 0.144$ meV was considered for both linear spin-wave theory and spin-wave theory with $1/S$ correction. The linear spin-wave theory simulation was performed using SpinW [48] program. The powder averaged spectrum was calculated using simple Monte Carlo integration with sampling size for each Q - E point set to 10^5 . Spin-wave theory with $1/S$ correction was calculated based on the results derived by Mourigal *et al.* [40]. The numerical integrations including powder averaging were implemented using the adaptive multidimensional integration (cubature) algorithm with the maximum number of integrated points set to 2×10^3 . Data in both cases were convoluted with estimated instrumental energy resolution $\Delta E = 0.025$ meV and Q resolution $\Delta Q = 0.015 \text{ \AA}^{-1}$ which was approximated by fitting the nuclear peak width. In order to make easier comparison between the simulated results and experimental data, we reduced the former into the same Q - E grid as the latter using spline interpolation.

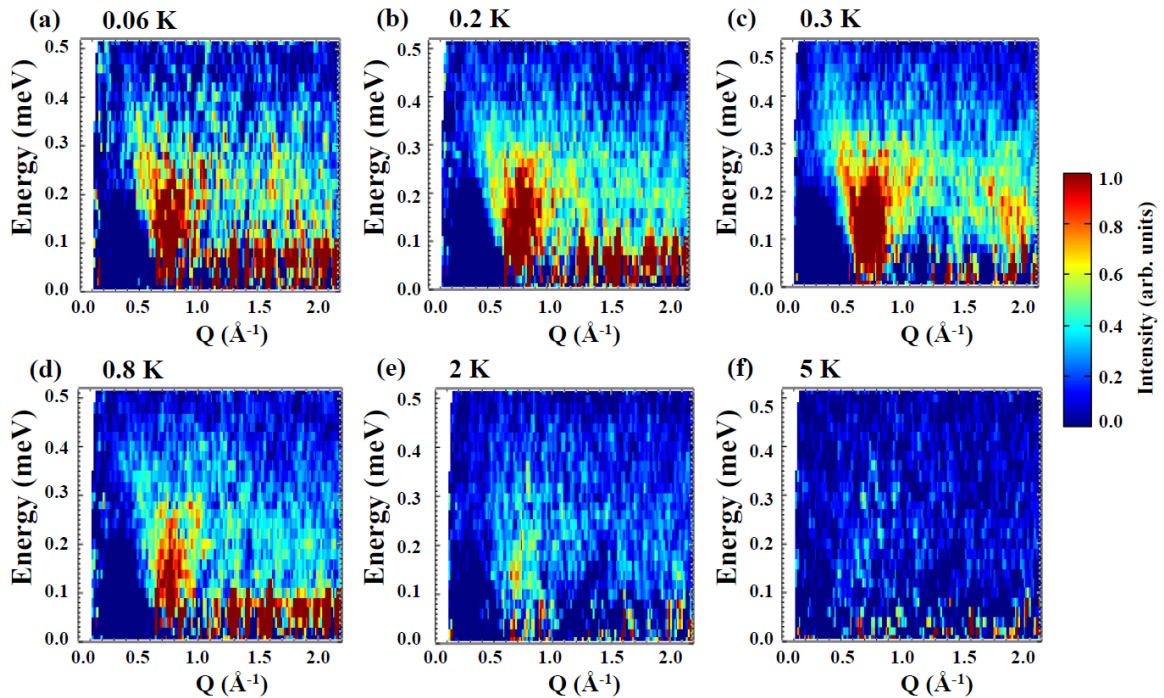


FIG. S2. (color online) The temperature dependence of INS spectra for $\text{Ba}_8\text{CoNb}_6\text{O}_{24}$. The back ground had been subtracted.